Inorganic Chemistry

Article

pubs.acs.org/IC

Sensitizing Tb(III) and Eu(III) Emission with Triarylboron Functionalized 1,3-Diketonato Ligands

Larissa F. Smith, Barry A. Blight, Hee-Jun Park, and Suning Wang*

Department of Chemistry, Queen's University, Kingston, Ontario K7M 3N6, Canada

Supporting Information

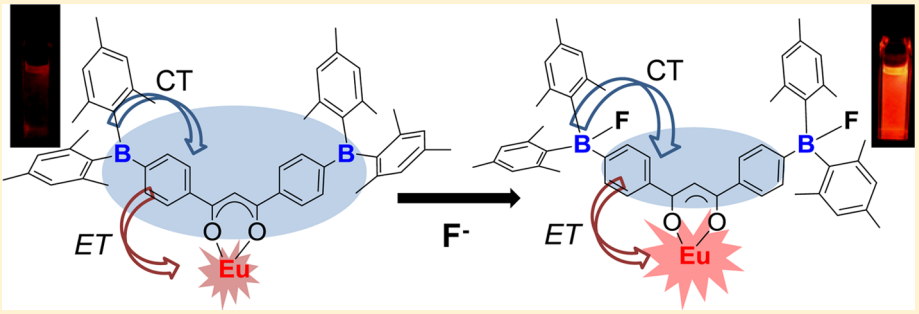

ABSTRACT: Four $BMes_2Ar$ (Mes = mesityl, Ar = phenyl or duryl) functionalized 1,3-diketonato ligands have been investigated for use in selective sensitization of Tb(III) and Eu(III) emission. These ligands have the general formula of $[R_1C(O)CR_2C(O)R_3]^-$ (R_1 = Ph, R_2 = H, R_3 = *p*-Ph-$BMes_2$, **L1**; R_1 = R_3 = *p*-Ph-$BMes_2$, R_2 = H, **L2**; R_1 = R_3 = Me, R_2 = *p*-Ph-$BMes_2$, **L3**; R_1 = R_3 = Me, R_2 = *p*-duryl-$BMes_2$, **L4**) and belong to class I (**L1** and **L2**) and class II (**L3** and **L4**), respectively. In class I, the boron unit is conjugated with the phenyl linker and the diketone backbone, while in class II, the boron unit, the linker unit, and the diketone unit are nonconjugated with a mutually orthogonal arrangement. To understand the impact of the location of the $BMes_2Ar$ unit on the electronic properties of the 1,3-diketone molecules and their ability in activating lanthanide emission, the difluoroboron chelate compounds (**1-BF_2** to **4-BF_2**) of ligands **L1**−**L4** were synthesized and examined. The class I ligands were effective in activating Eu(III) emission, while the class II ligands were effective in activating Tb(III) emission. Four Ln(III) complexes, **1Eu**, **2Eu**, **3Tb**, and **4Tb**, based on the **L1**−**L4** ligands, respectively, were prepared and examined. The emission quantum efficiency of **1Eu** and **2Eu** is low ($\Phi_{Eu} \leq 0.01$ in THF, 0.07−0.13 in the solid state), but can be greatly enhanced by the addition of fluoride ions. In contrast, the complex **4Tb** has a moderate emission efficiency (Φ_{Tb} = 0.14 in THF, 0.47 in the solid state) and experiences a distinct emission quenching upon the addition of fluoride. The selective sensitization of Eu(III) and Tb(III) by **L1**−**L4** and the distinct luminescent response of their Ln(III) complexes toward fluoride ions are caused by the distinct intraligand charge transfer transitions of the two different classes of ligands involving the $BMes_2$ unit.

INTRODUCTION

Luminescent lanthanide complexes have important applications in organic light-emitting diodes (OLEDs), sensors, and cellular imaging.[1−7] However, the emission intensity of lanthanide compounds is usually weak due to the low molar absorptivity that stems from the Laporte forbidden f−f transitions. Lanthanide emission can, however, be sensitized by appropriate ligands that can act as antennae to harvest photons and transfer the energy to the lanthanide via the ligand's triplet state.[8] Recently, we observed that triarylboron-functionalized carboxylate ligands (e.g., *p*-$BMes_2$-duryl-carboxylate) can be highly effective in selectively sensitizing Tb(III) or Eu(III) emission because the Mes → B (Ar-carboxylate) charge transfer (CT) transition has an appropriate triplet energy to stimulate luminescence from either Eu(III) or Tb(III).[9a] Furthermore, because of the ability of the triarylboryl unit to selectively bind to anions such as F^- or CN^-,[9b−d] the addition of F^- or CN^- to Eu(III) or Tb(III) complexes bearing the triarylboryl unit led to a distinct emission color change from either red (Eu(III)) or green (Tb(III)) to the characteristic blue fluorescence of the F^-- or CN^--bound $BMes_2Ar$-carboxylate ligand. This provided this class of compounds the potential as visual luminescent sensors/indicators for F^- or CN^-.[9a] Nonetheless, due to the lack of coordination saturation, lanthanide complexes based on monocarboxylate ligands have the tendency to form aggregates, oligomers, or polymers that are either highly prone to attack by external Lewis donors or insoluble in common solvents,[10] thus seriously limiting and complicating their applications. Therefore, to fully take advantage of the triarylboron unit in lanthanide compounds, it is necessary to replace the carboxylate binding unit with a ligand that has a stronger binding with the lanthanide ions than the aryl carboxylate ligands.

1,3-Diketones are a class of ligands that may be suitable for this purpose because lanthanide complexes based on 1,3-diketonato and derivative ligands are abundant, relatively stable,

Received: April 22, 2014
Published: July 11, 2014

   dx.doi.org/10.1021/ic500944t | *Inorg. Chem.* 2014, 53, 8036−8044

and commonly used in lanthanide-based luminescent materials.[1,8,11] On the basis of these considerations, we initiated the investigation on $BMes_2Ar$-functionalized 1,3-diketonato ligands in sensitizing lanthanide emission. We selected two classes of $BMes_2Ar$-functionalized 1,3-diketone ligands in the investigation. The first class of ligands (**L1** and **L2** in Scheme 1) has the

Scheme 1. Structures of the $BMes_2$-Functionalized 1,3-Diketones L1−L4 and the Synthetic Procedure of L2

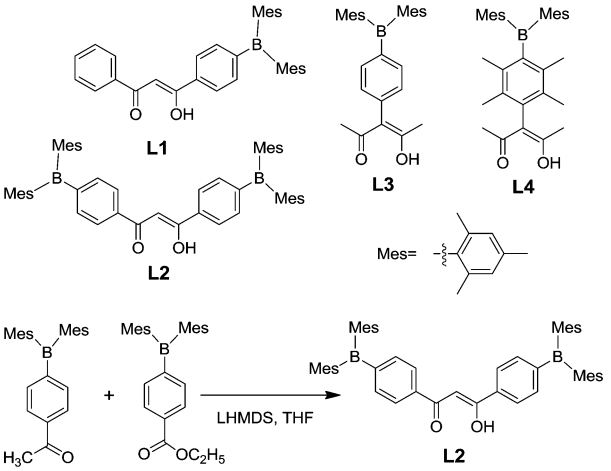

$BMes_2Ar$/Ar unit at the 1,3-position, while the second class (**L3** and **L4** in Scheme 1) has the $BMes_2Ar$ unit at the 2, or *meso*, position. The boron unit in class I ligands is expected to conjugate with the Ar linker and the diketone backbone, while that in class II is unlikely to conjugate with the linker and the diketone unit due to the orthogonal geometry imposed by steric interactions. This difference in geometry is expected to have a distinct impact on the CT transition, the T_1 energy, and the effectiveness of the ligands in sensitizing Ln(III) emission. Furthermore, these two classes of ligands are also expected to have a different response toward fluoride ions, leading to the possibility of further tuning the emission efficiency of the Ln(III) ion by fluoride ions, as illustrated in Chart 1.

To understand the impact of the ligands' geometry on their electronic properties and their possible impact on sensitizing Ln(III) emission, we first investigated the difluoroboron

Chart 1. Two Distinct Boryl-Functionalized 1,3-Diketone Systems and Their Possible Roles in Selective Sensitization/Tuning of Ln(III) Emission with the CT State and the Fluoride Ion

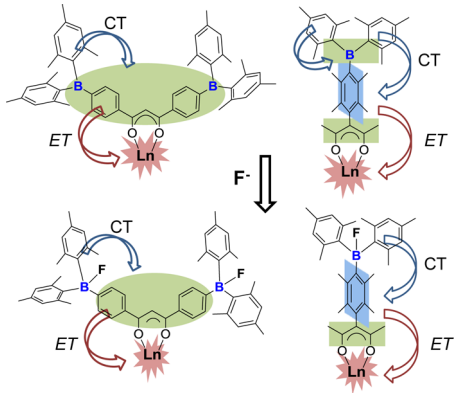

chelated compounds based on the $BMes_2Ar$-functionalized 1,3-diketone ligands, because the low energy electronic transitions of 1,3-diketonato difluoroboron compounds are known to be localized on the diketone unit.[12] This aspect of the work was also inspired by the recent discovery made by Fraser and co-workers on the effective use of difluoroboron 1,3-diketone compounds in hypoxia imaging and mechanoluminescence.[13] The results of our investigation revealed that the location of the $BMes_2Ar$ group and the nature of the Ar group have a distinct impact on the ability of the diketone ligands to sensitize Tb(III) or Eu(III) emission. The details are presented herein.

RESULTS AND DISCUSSION

Syntheses, Structures, and Electronic Properties of Ligands L1−L4 and Their BF_2-Chelated Compounds. Four $BMes_2Ar$ functionalized 1,3-diketone ligands, namely, **L1**, **L2**, **L3**, and **L4**, were synthesized. Ligand **L1** was prepared according to the previously known procedures.[14] Ligand **L2** was obtained by a Claisen condensation reaction between *p*-$BMes_2$-acetophenone and *p*-$BMes_2$-ethyl benzoate in the presence of 2.1 equiv of lithium hexamethyl disiliazide (LHMDS) in THF. *p*-$BMes_2$-acetophenone was prepared by a literature procedure,[13] while *p*-$BMes_2$-ethyl benzoate was prepared by the reaction of ethanol with *p*-$BMes_2$-benzoic acid in the presence of H_2SO_4. *p*-$BMes_2$-benzoic acid was prepared by lithiation of *p*-$BMes_2$-C_6H_4Br with *n*-BuLi, followed by the reaction with CO_2 and the subsequent quenching with HCl. During the course of our investigation on **L3** and **L4**, we became aware of the recent work by Thilagar and co-workers on the synthesis of **L3** and **L4** and their BF_2 chelate compounds (**3-BF_2** and **4-BF_2**).[12d] The synthetic procedures we used for **L3** and **L4** are similar to those reported by Thilagar. The BF_2-chelated compounds **1-BF_2** to **4-BF_2** of ligands **L1−L4** were prepared by the reaction of $BF_3(Et_2O)$ with the corresponding 1,3-diketone ligand, a procedure similar to that reported by Fraser and co-workers.[12a,b,13] Because **1-BF_2** and **2-BF_2** are new compounds, they were fully characterized by NMR, elemental, and single-crystal X-ray diffraction analyses. The crystal structures of **1-BF_2** and **2-BF_2** are shown in Figures 1 and 2, respectively. Two independent molecules are in the asymmetric unit of **1-BF_2**. One set of the **1-BF_2** molecules (containing the B3 and B4 atoms) have a parallel arrangement and form stacked dimers involving the central core, while the other set (containing the B1 and B2 atoms) are oriented at about a 60° angle with respect to the first set, forming F···H bonds with the CH_2Cl_2 solvent molecules (not shown in Figure 1). There are extensive F···H bonds and CH···π bonds in the crystal lattice of **1-BF_2**, some of which are highlighted Figure 1.

For **2-BF_2**, no stacked dimers were observed in the crystal lattice. There are, however, extensive $\pi\cdots\pi$ stacking, F···H bonds, and CH···π bonds involving the mesityl rings and the central core of the molecule. The crystal structures of **3-BF_2** and **4-BF_2** were reported previously.[12d] The difference between the structures of **1-BF_2** and **2-BF_2** and those of **3-BF_2** and **4-BF_2** is that the aryl linker is approximately coplanar with the 1,3-diketone unit in **1-BF_2** and **2-BF_2** but nearly orthogonal with the 1,3-diketone unit in **3-BF_2** and **4-BF_2**, as shown by the DFT optimized structures in Figure 3. It is noteworthy that the BC_3 plane has a much smaller dihedral angle with the phenyl linker in **1-BF_2** (~32°), **2-BF_2** (~32°), and **3-BF_2** (~24°) than it does with the duryl linker in **4-BF_2** (~58°). On the basis of the structural data, it is evident that the $BMes_2Ar$ group at the 2

dx.doi.org/10.1021/ic500944t | Inorg. Chem. 2014, 53, 8036−8044

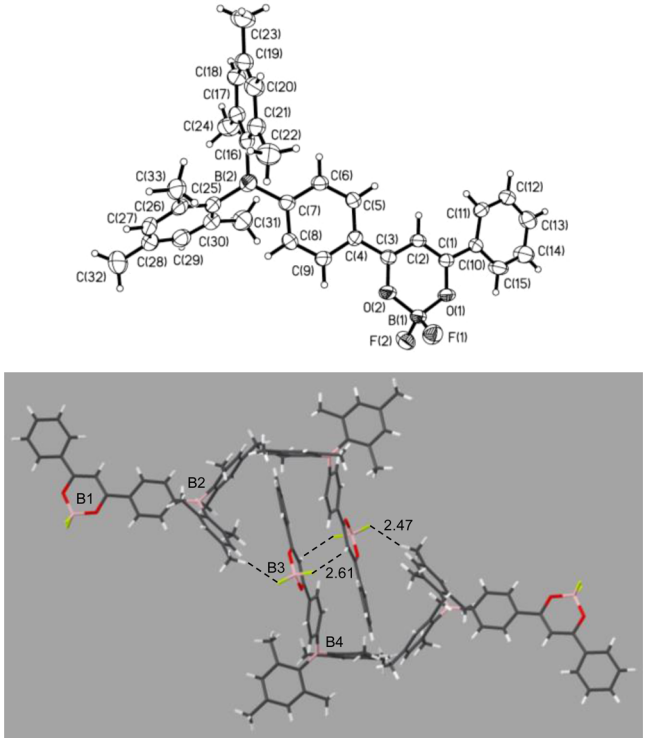

Figure 1. (Top) Crystal structure of one of the independent molecules of **1**-BF_2 with labeling schemes. (Bottom) Diagram showing the stacked pair and some of the F···H bonds. The CH_2Cl_2 solvent molecule was omitted for clarity.

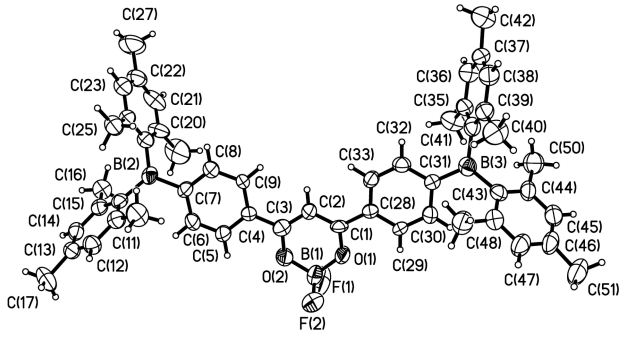

Figure 2. Crystal structure of **2**-BF_2 with labeling schemes.

position (the *meso* substitution) is not conjugated with the diketone unit, while that at the 1 and 3 positions has an extended conjugation with the 1,3-diketone unit. This should have a significant impact on the electronic properties and the triplet energies of these diketonato ligands.

For comparison, the photophysical properties of the BF_2-chelated compounds are summarized in Table 1. As shown by the absorption spectra and the fluorescence spectra in Figure 4, the four BF_2-chelated compounds indeed have considerably different absorption and fluorescence energies. The main absorption bands of **3**-BF_2 and **4**-BF_2 are similar in energy but are about 40−50 nm blue-shifted, compared to those of **1**-BF_2 and **2**-BF_2. Although **1**-BF_2 and **2**-BF_2 have the same number of phenyl rings conjugated with the diketone backbone, their absorption bands differ by about 15 nm. The extra $BMes_2$ group in **2**-BF_2 significantly lowers the energy of the absorption band and increases the extinction coefficient greatly, relative to that of **1**-BF_2.

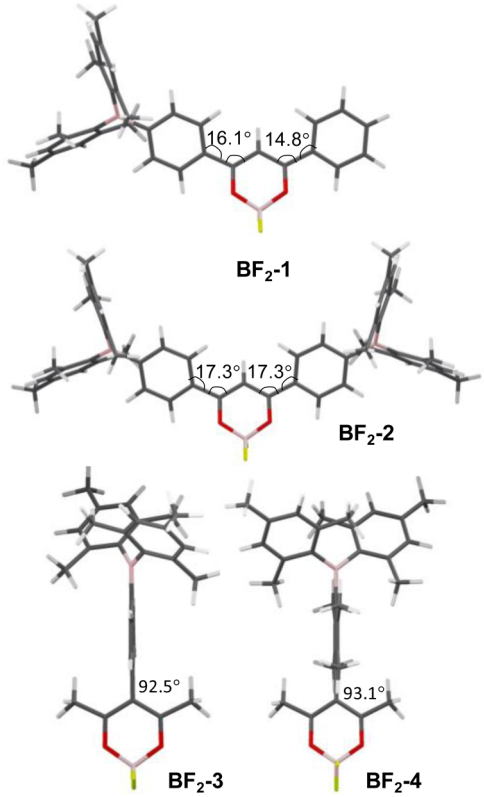

Figure 3. DFT optimized structures of **1**-BF_2 to **4**-BF_2 showing the torsion angle difference between the aryl linker and the 1,3-diketone unit in these molecules.

Table 1. Photophysical Properties of 1-BF_2 to 4-BF_2

compd	absorption λ_{max} (nm) (ε, 10^4 $M^{-1}cm^{-1}$)[a]	optical energy gap (nm)[b]	λ_{em} (nm)[1]/τ (ns)	Φ_{solu} /Φ_{ss}[c]
1-BF_2	379 (2.5)	430	424/1.55(3)	0.06/0.17
2-BF_2	394 (4.8)	450	446/1.87(4) 555/3.48(8)	0.04/0.12
3-BF_2	330 (1.7)	360	398	0.05/<0.01
4-BF_2	345 (1.8)	360	383	0.14/<0.01

[a]Recorded at ~1.0×10^{-5} M in CH_2Cl_2. [b]Determined from the absorption edge. [c]Solution quantum yields were determined using 9,10-diphenylanthracene as the reference, while the solid state quantum yields were determined using an integration sphere.

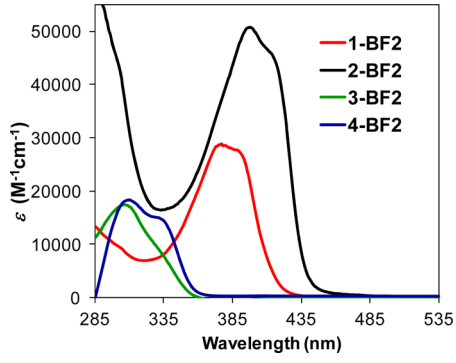

Figure 4. Absorption spectra of the BF_2-chelated compounds in CH_2Cl_2.

dx.doi.org/10.1021/ic500944t | Inorg. Chem. 2014, 53, 8036−8044

In the fluorescence spectra (Figure 5), **3-BF$_2$** and **4-BF$_2$** have a peak of λ_{max} = 398 and 383 nm, respectively. In contrast, the

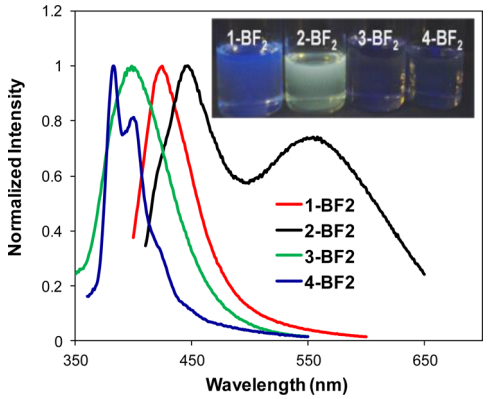

Figure 5. Fluorescence spectra of **1-BF$_2$** to **4-BF$_2$** at 1.0 × 10^{-5} M in CH_2Cl_2. (Inset) Photographs showing the emission colors of the same solutions under UV light (365 nm).

emission peak of **1-BF$_2$** and **2-BF$_2$** is considerably red-shifted to λ_{max} = 424 and 446 nm, respectively. Furthermore, **1-BF$_2$** and **2-BF$_2$** display a distinct concentration-dependent dual emission phenomenon (Supporting Information) with the second emission peak appearing as a broad band at λ_{max} = ∼535 nm for **1-BF$_2$** and ∼555 nm for **2-BF$_2$**. As a consequence of the dual emission, **1-BF$_2$** displays a yellowish white emission color at concentrations >1.0 × 10^{-3} M, while **2-BF$_2$** has a white emission color at concentrations >1.0 × 10^{-5} M in CH_2Cl_2. The relative intensity of the low-energy emission peak versus the high-energy emission peak increases with increasing concentration, an indication that the low energy emission band has an intermolecular origin. We attribute the low-energy emission peaks of **1-BF$_2$** and **2-BF$_2$** to excimer fluorescence because the decay lifetimes of these peaks is ∼3.5 ns, and a similar concentration-dependent dual emission phenomenon was reported previously,[15] for (dbm)**BF$_2$** (dbm = dibenzoylmethane) and derivatives in which the low-energy emission band at ∼550 nm was attributed to excimer fluorescence. The flat π-conjugated backbone of **1-BF$_2$** and **2-BF$_2$** as revealed by the crystal structures likely made these molecules prone to intermolecular interactions and excimer emission. **1-BF$_2$** was found to have a strong binding to fluoride ions with K = ∼7.5 × 10^6 M^{-1}, while **2-BF$_2$** displays a two-stage binding to fluoride ions with K_1 = ∼10^7 M^{-1} (Supporting Information).

From the time-dependent density functional theory (TD-DFT) computational data shown in Table 2, it can be seen that the calculated $S_0 \rightarrow S_1$ vertical excitation energy of the **BF$_2$** compounds matches well with the optical energy gap obtained from the absorption edge of the main absorption peak shown in Figure 4. The $S_0 \rightarrow S_1$ (and S_2 in **2-BF$_2$** due to degeneracy) state for **1-BF$_2$** and **2-BF$_2$** involves mainly the charge transfer transition from the Mes group to the π-conjugated backbone of the 1,3-diphenyldiketonato and the 3-coordinated boron atom (Figure 6), with little contributions from the **BF$_2$** unit, thus

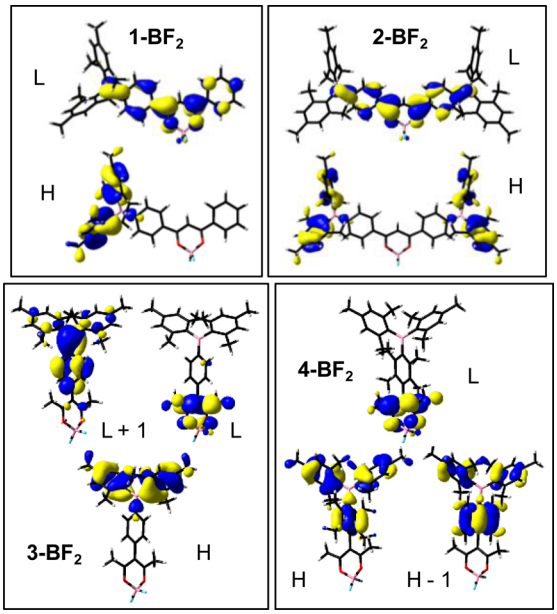

Figure 6. Key MO contributions in the $S_0 \rightarrow S_1$ transition of **1-BF$_2$** to **4-BF$_2$**, plotted with an isocontour value of 0.03. H = HOMO, L = LUMO.

validating the use of the **BF$_2$**-chelated compounds for the examination of the 1,3-diketonato ligands' electronic properties. In the case of **3-BF$_2$**, the transition to the S_1 state involves mixed Mes (π) → B-Ph (π^*) and Mes (π) → acac (π^*) CT transitions. In contrast, the S_1 transition in **4-BF$_2$** involves mainly Mes-duryl (π) → acac (π^*) CT transitions. The poor π-conjugation between the B atom, the linker, and the diketone unit in **3-BF$_2$** and **4-BF$_2$** due to the twisted arrangement of these units is responsible for the high $S_0 \rightarrow S_1$ transition energy of these molecules. The calculated $S_0 \rightarrow T_1$ transition energy follows the same order as that of $S_0 \rightarrow S_1$; **2-BF$_2$** has the lowest transition energy (19570 cm^{-1}), and **3-BF$_2$** has the highest (24040 cm^{-1}). The S_1–T_1 energy gap ($\Delta\nu$, cm^{-1}) follows the order of **1-BF$_2$** (2740) < **2-BF$_2$** (3050) < **3-BF$_2$** (3890) < **4-BF$_2$** (4340). These data illustrate that controlling the degree of π-conjugation between the $BMes_2$ unit and the linker-diketonato unit could lead to effective tuning of the T_1 energy and the S_1–

Table 2. TD-DFT Data of 1-BF$_2$ to 4-BF$_2$ and Experimental T$_1$ Energies of 1Gd to 4Gd

	TD-DFT Data				
	$S_0 \rightarrow S_1$		$S_0 \rightarrow T_1$	phosphorescence 77 K	
compd	contributions	E nm/cm^{-1}	E nm/cm^{-1}		$\lambda_{edge}/\lambda_{max}$ nm (cm^{-1})
1-BF$_2$	H → L (84%)	439/22780	499/20040	**1Gd**	480 (20800) /525 (19100)
2-BF$_2$	H → L (83%)	442/22620	511/19570	**2Gd**	505 (19800) /540 (18500)
3-BF$_2$	H → L+1 (76%)	358/27930	417/24040	**3Gd**	430 (23300) /470 (21300)
	H → L (24%)				
4-BF$_2$	H → L (31%)	361/27700	428/23360	**4Gd**	410 (24400) /450 (22200)
	H-1 → L (69%)				

dx.doi.org/10.1021/ic500944t | Inorg. Chem. 2014, 53, 8036–8044

Table 3. Photophysical Properties of Lanthanide Complexes

compd	λ_{ab}, nm ($\varepsilon \times 10^4$, M^{-1} cm^{-1})[a]	λ_{em}, nm[a]	Φ_{Ln}[b] (Φ_{ss})[c]	τ_{Ln} (μs) at 77 K
1Eu	270 (5.91), 370 (6.07)	425, 612	0.01 (0.13)	534
2Eu	325 (6.12), 390 (6.67)	440, 612	0.006 (0.07)	452
3Tb	316 (1.63)	393, 488, 546, 583	0.03 (0.31)	920
4Tb	323 (2.31)	489, 546, 583, 617	0.14 (0.47)	688

[a]Recorded in THF at ~1.0×10^{-5} M. [b]Determined in THF using cresyl violet as the reference in methanol (Φ = 0.54). [c]Determined using an integration sphere.

T_1 energy gap of the 1,3-diketonato ligands, hence the selective activation of Tb(III) and Eu(III) emission. Attempts to measure the T_1 energy of the BF_2-chelated compounds at 77 K were unsuccessful. The T_1 energy of the 1,3-diketonato ligands can, however, been experimentally determined using their Gd(III) complexes (see next section), and the data are listed in Table 2.

Syntheses and Luminescence of Tb(III) and Eu(III) Complexes. On the basis of the calculated T_1 energy of the $BMes_2Ar$-functionalized 1,3-diketone ligands (from the BF_2-chelated model compounds), **L1** and **L2** were expected to be unsuitable for sensitizing the emission of Tb(III) because their T_1 energy is below or similar to that of the emissive state $^5D_4$ (20 500 cm^{-1}) of Tb(III). However, they could be effective in sensitizing Eu(III) emission because their TD-DFT calculated T_1 energies are above those of the Eu(III) emissive state ($^5D_0$, 17 250 cm^{-1}) and the accepting state ($^5D_1$, 19 000 cm^{-1}), required for effective sensitization of Eu(III).[15] Indeed, we observed that **L1** and **L2** can sensitize Eu(III) emission but could not sensitize Tb(III) at all. Ligands **L3** and **L4** were expected to be effective in activating Tb(III) emission, and possibly Eu(III) as well, because of their high T_1 energy. However, we observed that **L3** and **L4** are only capable of sensitizing the Tb(III) ion and are not effective at all in sensitizing Eu(III) emission. Our investigation therefore focused on the complexes of Eu-**L1** (**1Eu**), Eu-**L2** (**2Eu**), Tb-**L3** (**3Tb**), and Tb-**L4** (**4Tb**). The Ln(III) complexes were prepared by the reaction of the corresponding ligand with $LnCl_3(H_2O)_6$ in a 3:1 ratio in the presence of a base. To saturate the coordination sphere of the Eu(III) ion in **1Eu** and **2Eu**, 1,10-phenanthroline, which has a T_1 energy of ~20 800 cm^{-1} was added. Compound **1Eu** with the formula of $Eu(L1)_3(phen)(H_2O)_{1.5}$ was isolated and characterized by ^1H NMR and elemental analysis. For **2Eu**, however, repeated attempts only led to the isolation of a compound with the composition of $Eu(L2)_3(H_2O)_{10}$. The lack of phen coordination to the Eu(III) ion may be attributed to the large size of **L2**. It is well-known that to sensitize the emission of Tb(III), the T_1 energy of the surrounding ligands needs to be ~3000 cm^{-1} higher than the $^5D_4$ state.[16] Therefore, chelate ligands such as bpy and phen are not suitable for use in Tb(III) compounds because their low T_1 state[17] can deactivate the Tb(III) emission. In an attempt to saturate the coordination sphere of the Tb(III) ion, we added a large excess of trioctylphosphine oxide (TOPO) in the synthesis of **3Tb** and **4Tb**. However, NMR and elemental analyses indicated that TOPO is not present in the Tb(III) compounds. Instead, the vacant coordination sites in **3Tb** and **4Tb** appear to be occupied by H_2O molecules, giving these two complexes formulas of $Tb(L3)_3(H_2O)_8$ and $Tb(L4)_3(H_2O)_9$, respectively, on the basis of elemental analysis data.

The absorption and luminescent data of the lanthanide complexes are summarized in Table 3. Complex **1Eu** displays a bright red luminescence in the solid state (Figure 7) with Φ_{Eu} = 0.13. In solution, however, **1Eu** emits weakly with Φ_{Eu} = ~0.01,

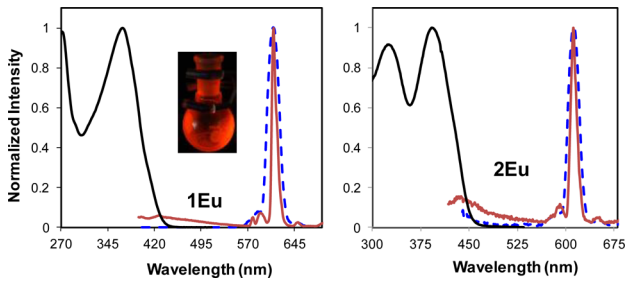

Figure 7. Normalized (black line) absorption and (red line) emission spectra of (left) **1Eu** and (right) **2Eu** in THF and (dashed blue line) the solid state with λ_{ex} = 380 and 395 nm, respectively. (Inset) Photograph showing the bright red emission color of **1Eu** in the solid state.

which may be attributed to the interactions with the solvent molecules (e.g., THF). Nonetheless, the energy transfer from ligand **L1** to the Eu(III) ion appears to be efficient because the ligand's fluorescent peak at ~420 nm is fairly weak in the emission spectrum of **1Eu** in THF and is not detectable in the solid state. Compared to that of **1Eu**, the emission of **2Eu** is much weaker with Φ_{Eu} < 0.01 in THF and Φ_{Eu} = 0.07 in the solid state. Furthermore, the ligand's fluorescent peak contributes significantly to the emission spectrum, an indication that the energy transfer from **L2** to the Eu(III) ion in **2Eu** is much less efficient than **L1** in **1Eu**. Both complexes **3Tb** and **4Tb** display bright green emissions in the solid state with very impressive emission quantum efficiencies (Φ_{Tb} = 0.31 and 0.47, respectively). The fluorescent peaks of **L3** and **L4** do not contribute to the emission spectra of **3Tb** and **4Tb** in the solid state (Figure 8), supporting a highly efficient energy transfer from the ligand to the Tb(III) center in these two compounds. In solution, however, the Tb(III) emission from **3Tb** is much

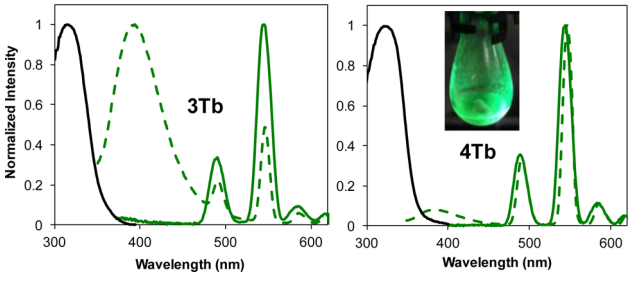

Figure 8. Normalized (black line) absorption and (dashed green line) emission spectra of (left) **3Tb** and (right) **4Tb** in THF and (solid green line) the solid state with λ_{ex} = 323 and 330 nm, respectively. (Inset) Photograph showing the bright green emission color of **4Tb** in the solid state.

dx.doi.org/10.1021/ic500944t | Inorg. Chem. 2014, 53, 8036−8044

weaker (Φ_{Tb} = 0.03 in THF), and the emission spectrum is dominated by the fluorescent peak of **L3** at 393 nm, as shown in Figure 8. Although the Tb(III) emission from **4Tb** is also much less efficient in THF, compared to that in the solid state, it retains a moderate emission quantum efficiency (Φ_{Tb} = 0.14) with a much smaller ligand fluorescence contribution in the emission spectrum in THF, compared to that of **3Tb**. The consistently high Tb(III) emission efficiency of **4Tb**, relative to that of **3Tb**, supports the observation that **L4** is much more effective than **L3** in sensitizing Tb(III) emission. The much-reduced emission quantum efficiency of **3Tb** and **4Tb** in solution is most likely caused by the dynamic dissociation/association of H_2O molecules and the solvent molecules around the Tb(III) center. To gain a better understanding of the difference of **L1**−**L4** in sensitizing Eu(III) and Tb(III) emission, we prepared the Gd(III) compounds **1Gd**−**4Gd** without the use of the phen ligand so that the T_1 energy of **L1**−**L4** can be determined. The phosphorescent spectra of **1Gd**−**4Gd** were recorded at 77 K. The T_1 energies of these compounds were estimated using the emission edge (λ_{edge}) of the phosphorescent peak, as shown in Figure 9, and the data are listed in Table 2 for comparison with the TD-DFT calculated T_1 energies of the BF_2-chelated compounds.

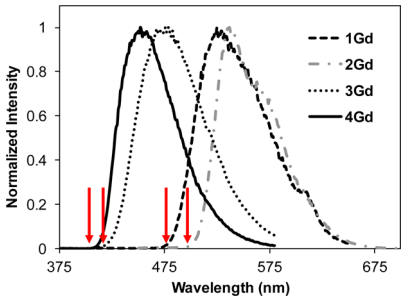

Figure 9. Phosphorescent spectra of Gd(III) compounds recorded at CH_2Cl_2 at 77 K. The red arrows indicate the emission edge (λ_{edge}).

The experimental T_1 energy of the ligands obtained from the phosphorescent spectra of the Gd(III) compounds follows the order of **L4** > **L3** > **L1** > **L2**. The observed T_1 energies and their trends for **L1** and **L2** agree well with those calculated for **1**-BF_2 and **2**-BF_2, while the observed T_1 energy trend of **L3** and **L4** is opposite of that calculated for **3**-BF_2 and **4**-BF_2. To determine whether this was caused by the solvent, we repeated TD-DFT calculations for **1**-BF_2, **3**-BF_2, and **4**-BF_2 by introducing the solvent parameter (CH_2Cl_2). The T_1 energies obtained in this manner are slightly lower in energy but follow the same order as those obtained without including the solvent effect (Supporting Information). This indicates that the BF_2-chelated compounds are not perfect as model compounds for the elucidation of the triplet energy of the lanthanide complexes. The poor sensitization of Eu(III) emission by **L2** could be explained by the relatively small energy difference between the T_1 state of **L2** and the $^5D_0$ state of Eu(III) ($\Delta\upsilon$ = 2550 cm^{-1}), because the effective sensitization of Eu(III) requires $\Delta\upsilon \geq$ ~3000 cm^{-1}.[16] The fact that **L3** and **L4** are not effective in sensitizing Eu(III) emission may be attributed to their high T_1 energies, which are more than 6000 cm^{-1} above the $^5D_0$ state and known to cause Φ_{Eu} decrease.[16,18] The highly twisted geometry of the *meso*-substituted **L3** and **L4** ligands is clearly responsible for their high T_1 energy and their ability to sensitize Tb(III) emission, compared to the planar **L1** and **L2** ligands. The T_1 state of **L4** is 3900 cm^{-1} above the Tb(III) emissive state $^5D_4$, which is greater than the required 3000 cm^{-1} threshold for effective Tb(III) sensitization, while that of **L3** is only ~2800 cm^{-1} above the threshold, which explains the more effective sensitization of the Tb(III) ion by **L4**. The high T_1 energy of **L4**, relative to that of **L3**, is caused by the greater steric congestion imposed by the duryl ring in **L4**. The intraligand charge transfer transition involving the $BMes_2$ unit in **L3** and **L4**, as established by the model compound **4**-BF_2 (Figure 6), is believed to play a key role in sensitizing the Tb(III) emission in **3Tb** and **4Tb** because a *meso*-duryl-acac ligand that lacks the $BMes_2$ unit was not effective at all in sensitizing Tb(III) emission (Supporting Information).

Tuning the T_1 Energy and the Emission Efficiency of Eu(III) and Tb(III) with Fluoride Ions. To further examine the roles of the $BMes_2$ group in sensitizing Eu(III) and Tb(III) emission by **L1** and **L4**, we performed fluoride titration experiments for **1Eu, 2Eu**, and **4Tb**. The tetrabutylammonium fluoride (TBAF) titration experiment for **3Tb** was not performed because the fluoride ions were expected to further deactivate the Tb(III) emission in **3Tb** due to the decrease of the T_1 energy of the fluoride adduct (Supporting Information). The addition of TBAF to the solution of **1Eu** led to a great increase of the Eu(III) emission peak and the Φ_{Eu} from ~0.01 to ~0.23 in THF (Figure 10), and the ligand's fluorescence was

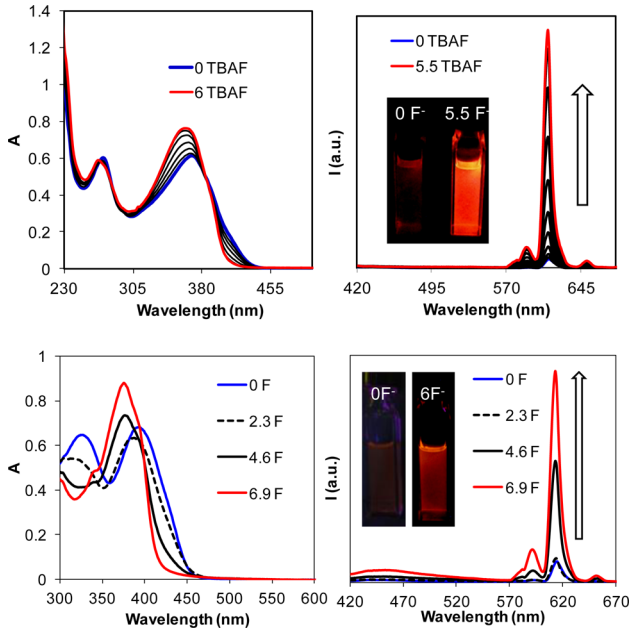

Figure 10. (Left) Absorption and (right) emission spectral changes of (top) **1Eu** and (bottom) **2Eu** with the addition of TBAF in THF.

not observed. In the absorption spectrum of **1Eu**, the absorption band at ~370 nm experienced a blue shift as the absorption edge shifted from 440 to 410 nm, which may be explained by the LUMO level (π^*) of **L1** having a large contribution from the B atom and the F^- binding to the B center would remove the B atom contribution to the π^* level, thus raising the LUMO and the $S_0 \rightarrow S_1$ transition energy ($BMes_2F$ to the chelate backbone CT transition). The T_1 energy of the fluoride adduct **1Gd**−**F** was determined to be at 460 nm/21700 cm^{-1} (Supporting Information), which is ~900 cm^{-1} higher than that of **1Gd** and is likely responsible for the more effective sensitization of the Eu(III) ion. After the

dx.doi.org/10.1021/ic500944t | Inorg. Chem. 2014, 53, 8036−8044

addition of ~6 equiv of TBAF, the absorption and emission spectral change of **1Eu** with fluoride could be reversed by the addition of water, an indication that **1Eu** remained intact under this condition. The addition of up to ~2 equiv of TBAF to **2Eu** led to no significant change of the emission spectrum but a small blue shift of the absorption peak at 400 nm, which may be attributed to the interaction of the fluoride ion with the H_2O molecules associated with the complex.[9c] Further addition of TBAF led to a further blue shift of the absorption spectrum and a great increase of the Eu(III) emission intensity (Figure 10) and the emission quantum efficiency (from ~0.006 to 0.06), which can be attributed to the binding of the fluoride ion to the B center in **L2** that increases the T_1 energy of the ligand, resulting in more effective sensitization of the Eu(III) emission. This is corroborated by the T_1 energy of **2Gd** that is shifted from 505 nm (19 800 cm^{-1}) to 490 nm (20 400 cm^{-1}) with 3 equiv of TBAF, and to 480 nm (20800 cm^{-1}) with >6 equiv of TBAF (Supporting Information), which is more than 3000 cm^{-1} above the $^5D_0$ state of Eu(III). For both **1Eu** and **2Eu**, the addition of a large excess of TBAF led to the dissociation of the diketonato ligands because the Eu(III) emission intensity of the complexes experienced an irreversible decrease. For **4Tb**, the addition of TBAF led to a great increase of the absorption band at λ_{max} = 330 nm and the appearance of a weak low energy band at 400−450 nm in the absorption spectrum (Figure 11). The

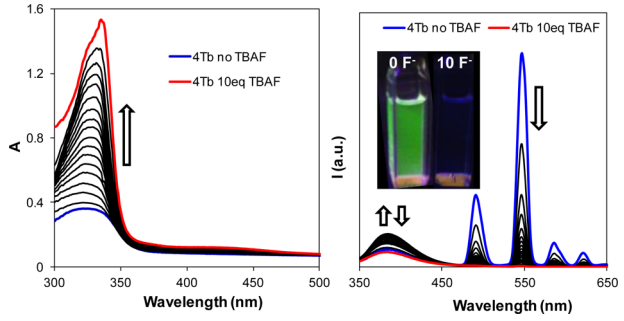

Figure 11. (Left) Absorption and (right) emission spectral change of **4Tb** with the addition of TBAF in THF.

new low energy absorption band may be attributed to the [$BMes_2$(duryl)F] → acac CT transition. This could be explained by the fact that the B atom has no contribution to the LUMO level (π^*) in **L4**; thus, the F^- binding to the B center would not significantly alter the energy of LUMO; instead, it would destabilize the HOMO and HOMO+1 (Figure 6), leading to a decrease of the $S_0 \rightarrow S_1$ transition energy. In the emission spectrum of **4Tb**, a gradual quenching of the Tb(III) emission peaks was observed with the addition of TBAF. The fluorescent peak of **L4** gained intensity with the addition of up to ~5 equiv of TBAF, which is similar to the behavior of **4-BF_2**,[12d] thus supporting the binding of F^- to the B center. The T_1 energy of **4Gd** was found to shift from 410 nm (24 400 cm^{-1}) to ~420 nm (23 800 cm^{-1}) with the addition of TBAF (Supporting Information). The absorption and emission spectral change of **4Tb** with TBAF could not be reversed by the addition of water, an indication that the fluoride ions likely caused an irreversible dissociation of the **L4** ligand on **4Tb**. Thus, the quenching of Tb(III) emission in **4Tb** by TBAF could be attributed to both the T_1 energy decrease and the dissociation of **L4** from the Tb(III) center. The coordination unsaturation of **4Tb** is most likely responsible for the facile dissociation of the chelate ligands in the presence of fluoride ions.

CONCLUSIONS

We have illustrated that the location of the $BMes_2Ar$ unit on the 1,3-diketonato ligand has a dramatic impact on the T_1 energy of the ligand and its ability to sensitize Eu(III) or Tb(III) emission. The *meso*-substitution by a $BMes_2Ar$ group provides the ligand a high T_1 energy that leads to the effective sensitization of Tb(III) emission. When the Ar group is highly sterically demanding, such as a duryl ring, the *meso*-substituted 1,3-diketonato ligand is the most effective in sensitizing Tb(III) emission. In addition, the CT transition involving the $BMes_2$-duryl unit has been found to play a key role in activating Tb(III) emission. The addition of fluoride ions to Tb(III) compounds that contain the *meso*-substituted 1,3-diketonato ligands leads to a decrease of the T_1 energy and the quenching of the Tb(III) emission. The substitution by a $BMes_2Ar$ group at the 1,3-positions of the diketonato ligand results in a relatively low T_1 energy of the ligand, which is only moderately effective in sensitizing Eu(III) emission. However, the addition of fluoride ions can significantly increase the T_1 energy and greatly enhance the Eu(III) emission efficiency based on the 1,3-substituted ligands. The most effective ligand for Eu(III) emission sensitization has been found to be the mono-$BMes_2$ substituted 1,3-diphenyldiketonato ligand and its fluoride adduct. This work demonstrates the use and the potential of triarylboryl-functionalized ligands in selective activation of Ln(III) emission and the tuning of Ln(III) emission efficiency. Although the $BMes_2Ar$-functionalized 1,3-diketonato ligands provide a much better stability to the Ln(III) complexes than the previously reported $BMes_2Ar$-functionalized monocarboxylate ligands do, the Ln(III) complexes based on this class of ligands are still vulnerable to ligand replacement by fluoride ions, thus limiting their use as sensors for fluoride ions.

EXPERIMENTAL SECTION

General. All reagents, unless otherwise specified, were received from Sigma-Aldrich and used without further purification. Elemental analyses were performed by the analytical laboratories at the University of Montreal. The UV−visible spectra were obtained on a Varian Cary 50 UV−visible spectrophotometer. Excitation and emission spectra were recorded on a Photon Technologies International QuantaMaster model 2 spectrometer. Luminescent decay lifetimes were measured on a Photon Technology International Phosphorescent lifetime spectrometer, Timemaster C-631F, equipped with a xenon flash lamp and a digital emission photon multiplier tube for both excitation and emission. All solutions for photophysical data measurements were degassed under a nitrogen atmosphere. Solution emission quantum yields were determined using optically dilute solutions ($A \approx 0.1$), 9,10-diphenylanthracene in ethanol (ϕ = 0.95) as the standard for the ligands and creysol violet in methanol (ϕ = 0.54) for the lanthanide complexes in degassed and distilled CH_2Cl_2 or THF at 298 K. The DFT calculations were performed using the Gaussian09, revision B.01,[19] software package and the High Performance Computing Virtual Laboratory (HPCVL) at Queen's University. The ground-state geometries were fully optimized at the B3LYP level using the 6-311+G(d,p) basis set[20] for all atoms. TD-DFT calculations were performed to obtain the singlet and triplet excitation energies. Fluoride titrations were performed by using tetrabutylammonium fluoride (TBAF) as a fluoride source. 1-(4-(dimesitylboryl)phenyl)ethanone and ligands **L1**, **L3**, **L4**, **3-BF_2**, and **4-BF_2** were synthesized according to previously reported procedures.[12d]

Synthesis of L2. This compound was obtained by a three-step procedure:

dx.doi.org/10.1021/ic500944t | Inorg. Chem. 2014, 53, 8036−8044

(1) Synthesis of 4-Dimesitylboryl Benzoic Acid. A solution of 1.00 g of 1-bromo-4-dimesitylborylphenyl (2.47 mmol) in 30 mL of THF was cooled to −78 °C, and 1.6 M *n*-BuLi (1.7 mL, 2.71 mmol) was added dropwise. After the mixture was stirred for 1 h, a CO_2 filled balloon was vented into the mixture, the mixture was allowed to warm slowly to ambient temperature, and it was kept overnight. Then, 2 M HCl was added to quench the reaction, and the product was extracted into diethyl ether. The product was then was washed with water and dried with $MgSO_4$. The solvent was removed under reduced pressure, and the product was washed with hexanes; 0.65 g of the product was obtained as a white solid (70% yield). ^{1}H NMR (300 MHz, 298 K, $CDCl_3$, δ, ppm): 8.10 (d, J = 7.4 Hz, 2H), 7.62 (d, J = 7.4 Hz, 2H), 6.86(s, 4H), 2.33 (s, 6H), 2.01 (s, 12H).

(2) Synthesis of 4-Dimesitylboryl Benzoic Acid Ethyl Ester. 4-Dimesitylboryl benzoic acid (310 mg, 0.80 mmol) was dissolved in 75 mL of absolute ethanol, and the solution was heated to reflux. Three drops of concentrated H_2SO_4 was added, and the mixture was refluxed overnight. Then, the product was extracted by diethyl ether, washed with water, and dried with $MgSO_4$. The product was further purified by column chromatography using CH_2Cl_2 as the eluent (310 mg, 93%). ^{1}H NMR (300 MHz, 298 K, $CDCl_3$, δ, ppm): 8.05 (d, J = 7.9 Hz, 2H), 7.62 (d, J = 7.9 Hz, 2H), 6.86 (s, 4H), 4.41 (q, J = 7.0 Hz, 2H), 2.33 (s, 6H), 2.03 (s, 12H), 1.41 (t, J = 7.0 Hz, 3H).

(3) Synthesis of L2. 4-Dimesitylboryl benzoic acid ethyl ester (310 mg, 0.75 mmol), 1-(4-(dimesitylboryl)phenyl)ethanone (265 mg 0.75 mmol), and lithium hexamethyl disiliazide (LHMDS) (264 mg, 1.58 mmol) were dissolved in 10 mL of THF and stirred for 1 h at ambient temperature. The mixture was then refluxed for 3 h and allowed to stir at ambient temperature for another 40 h. Ammonium chloride was added, and the product was extracted into diethyl ether, washed with water, and dried with $MgSO_4$. The crude mixture was purified by column chromatography using CH_2Cl_2 as the eluent, producing **L2** (251 mg, 47% yield). ^{1}H NMR (300 MHz, 298 K, $CDCl_3$, δ, ppm): 16.90 (s, 1H), 7.99 (d, J = 8.1 Hz, 4H), 7.67 (d, J = 8.1 Hz, 4H), 6.97 (s, 1H), 6.89(s, 8H), 2.36 (s, 12H), 2.05 (s, 24H).

Synthesis of BF_2 Complexes. All BF_2-chelated complexes were synthesized in a similar fashion. Typically, 1 equiv of the diketonato ligand was reacted with 2.1 equiv of $BF_3{\cdot}OEt_2$ in refluxing CH_2Cl_2, and the product was purified by column chromatography using CH_2Cl_2 as the eluent.

***1*-BF_2.** 32% yield. ^{1}H NMR (400 MHz, 298 K, $CDCl_3$, δ, ppm): 8.17 (d, J = 7.9 Hz, 2H), 8.10 (d, J = 7.9 Hz, 2H), 7.72 (t, J = 7.4, 1H), 7.67 (d, J = 8.1 Hz, 2H), 7.58 (dd, J = 8.1 Hz, J = 7.4 Hz, 2H), 7.24 (s, 1H), 6.86 (s, 4H), 2.34 (s, 6H), 2.00 (s, 12H). ^{13}C NMR (100 MHz, 298 K, $CDCl_3$, δ, ppm): 183.50, 183.15, 140.92, 139.63, 135.85, 135.37, 134.05, 132.00, 129.23, 129.00, 128.46, 128.17, 115.63, 93.93, 23.45, 21.25. ^{11}B NMR (128 MHz, 298 K, $CDCl_3$, δ, ppm): 1.35. ^{19}F NMR (376 MHz, 298 K, $CDCl_3$, δ, ppm): −140.50. Anal. Calcd for $C_{33}H_{32}B_2F_2O_2$: C, 76.19; H, 6.20. Found: C, 73.45; H, 6.34. This can be attributed to 0.3 CH_2Cl_2, which is corroborated by the crystal structural data. Anal. Calcd for $C_{33.3}H_{32.6}B_2Cl_{0.6}F_2O_2$: C, 73.29; H, 6.02.

***2*-BF_2.** 48% yield. ^{1}H NMR (400 MHz, 298 K, CD_2Cl_2, δ, ppm): δ 8.12 (d, J = 8.3 Hz, 4H), 7.66 (d, J = 8.3 Hz, 4H), 7.33 (s, 1H), 6.86 (s, 4H), 2.32 (s, 6H), 1.99 (s, 12H). ^{13}C NMR (100 MHz, 298 K, CD_2Cl, δ, ppm): 183.93, 141.45, 140.25, 136.43, 134.61, 128.97, 128.82, 95.24, 23.78, 21.56. ^{11}B NMR (128 MHz, 298 K, CD_2Cl_2, δ, ppm): 1.30. ^{19}F NMR (376 MHz, 298 K, CD_2Cl_2, δ, ppm): −140.60. Anal. Calcd for $C_{51}H_{53}B_3F_2O_2$: C, 79.72; H, 6.95. Found: C, 78.87; H, 7.14. This can be attributed to 0.5 H_2O. Anal. Calcd for $C_{51}H_{54}B_3F_2O_{2.5}$: C, 78.79; H, 7.00.

Synthesis of 1Eu. Ligand **L1** (36 mg, 0.075 mmol) and 1,10-phenanthroline (4.4 mg, 0.025 mmol) were suspended in EtOH (2 mL), NaOH (1 M aqueous solution, 3 equiv) was added, and the mixture became a bright yellow solution. $EuCl_3{\cdot}6H_2O$ (9 mg, 0.025 mmol) dissolved in 1 mL of EtOH was added dropwise to the reaction mixture. A pale yellow precipitate formed quickly after the mixture was stirred at ambient temperature for 10 min. The reaction mixture was then warmed to 60 °C and stirred for another 3 h. After the reaction mixture was cooled to 0 °C and stirred for 10 min, the product was isolated by a vacuum filtration as a yellow solid, which was further purified by dissolving in CH_2Cl_2, followed by precipitation by the addition of cold ethanol (27 mg, 62% yield). ^{1}H NMR (400 MHz, 298 K, $CDCl_3$, δ, ppm): 10.91 (d, J = 7.9 Hz, 2H), 10.49 (br, 2H), 9.85 (br, 2H), 8.90 (d, J = 7.9 Hz, 2H), 6.91−6.71 (m, 27H), 6.41 (br, 6H), 5.45 (s, 6H), 2.30 (s, 18H), 1.82 (s, 36H). Anal. Calcd for $C_{111}H_{104}B_3O_6N_2Eu$: C, 76.34; H, 6.00; N 1.60. Found: C, 75.11; H, 5.84; N, 1.41. This can be attributed to 1.5 H_2O. Anal. Calcd for $C_{111}H_{107}B_3O_{7.5}N_2Eu$: C, 75.18; H, 6.08; N, 1.58.

Synthesis of 2Eu. First, 50 mg of **L2** (0.069 mmol, 3 equiv) and 6.3 mg of phenanthroline (0.023 mmol, 1.5 equiv) were suspended in 6 mL of absolute ethanol. Then, potassium *t*-butoxide (0.06 mL, 1 M in THF, 3 equiv) was added dropwise to this suspension. Afterward, 8.5 mg of $EuCl_3{\cdot}6H_2O$ dissolved in a 4 mL of absolute ethanol was added dropwise to the ligand solution, and a yellow precipitate formed immediately. The mixture was stirred overnight in a warm water bath, filtered, and washed with H_2O and ethanol. **2Eu** (32 mg) was isolated as a yellow powder (58% yield). ^{1}H NMR (400 MHz, 298 K, $CDCl_3$, δ, ppm): 10.93 (br), 10.58 (br), 8.66 (br), 6.84−6.76 (m), 2.29 (s), 1.92 (s). Anal. Calcd for $C_{153}H_{179}B_6Eu_1O_{16}$ ($[Eu(L2)_3(H_2O)_{16}]$): C, 73.77; H, 7.24. Found: C, 74.31; H, 6.74.

Synthesis of 3Tb and 4Tb. These two compounds were synthesized by the same procedure. The 1,3-diketone ligand (3 equiv) and trioctylphosphine oxide (3 equiv) were mixed in ethanol. NaOH (1 M aqueous solution, 3 equiv) was added dropwise, and the mixture was allowed to stir at room temperature until the ligand was completely dissolved. $TbCl_3{\cdot}6H_2O$ (1 equiv) dissolved in ethanol was added dropwise to the ligand solution, and a white precipitate formed immediately. The mixture was stirred for 3 h at ambient temperature, and the precipitate was collected, redissolved in CH_2Cl_2, washed with water, and reprecipitated by the addition of ethanol.

3Tb *($Tb(L3)_3(H_2O)_8$).* 32% yield. Anal. Calcd for $C_{87}H_{112}B_3O_{14}Tb$: C, 66.42; H, 7.18. Found: C, 66.50; H, 7.25.

4Tb *($Tb(L4)_3(H_2O)_9$).* 34% yield. Anal. Calcd for $C_{99}H_{140}B_3O_{16}Tb$: C, 67.23; H, 8.38. Found: C, 67.04; H, 7.51.

X-ray Crystallographic Analysis. Single crystals of **1**-BF_2 and **2**-BF_2 were mounted on glass fibers and were collected on a Bruker Apex II single-crystal X-ray diffractometer with graphite-monochromated Mo Kα radiation, operating at 50 kV, 30 mA, and 180 K. Data were processed on a PC with the aid of the Bruker SHELXTL software package (version 6.10)[21] and corrected for absorption effects. The crystals of **1**-BF_2 and **2**-BF_2 belong to the triclinic space group $P\bar{1}$ and the monoclinic crystal space group $P2_1$, respectively. There are two independent molecules of **1**-BF_2 and one CH_2Cl_2 solvent molecule in the asymmetric unit of **1**-BF_2. All non-hydrogen atoms were refined anisotropically. Complete crystal structure data can be found in the Supporting Information. The crystal data of **1**-BF_2 and **2**-BF_2 have been deposited at the Cambridge Crystallographic Data Center (CCDC 992479 and 992480, respectively).

■ ASSOCIATED CONTENT

Ⓢ Supporting Information

NMR spectra, concentration-dependent fluorescence spectra, and fluoride titration data of **1**-BF_2 and **2**-BF_2; computational data, phosphorescent spectra of Gd(III) compounds and their fluoride adducts, and crystal structural data. This material is available free of charge via the Internet at http://pubs.acs.org.

■ AUTHOR INFORMATION

Corresponding Author

*E-mail: wangs@chem.queensu.ca.

Notes

The authors declare no competing financial interest.

■ ACKNOWLEDGMENTS

We thank the Natural Sciences and Engineering Research Council of Canada for financial support and Dr. Ian Wyman for

his assistance in some of the fluoride binding constant calculations.

REFERENCES

(1) (a) De Bettencourt-Dias, A. *Dalton Trans.* **2007**, 2229−2241. (b) Kido, J.; Okamoto, Y. *Chem. Rev.* **2002**, *102*, 2357−2368. (c) Wang, J.; Wang, R.; Yang, J.; Zheng, Z.; Carducci, M. D.; Cayou, T.; Peyghambarian, N.; Jabbour, G. E. *J. Am. Chem. Soc.* **2001**, *123*, 6179−6180.

(2) Cable, M. L.; Kirby, J. P.; Gray, H. B.; Ponce, A. *Acc. Chem. Res.* **2013**, *46*, 2576−2584.

(3) Dennison, G. H.; Sambrook, M. R.; Johnston, M. R. *Chem. Commun.* **2014**, *50*, 195−197.

(4) Comby, S.; Tuck, S. A.; Truman, L. K.; Kotova, O.; Gunnlaugsson, T. *Inorg. Chem.* **2012**, *51*, 10158−10168.

(5) (a) Tsukube, H.; Shinoda, S. *Chem. Rev.* **2002**, *102*, 2389−2403. (b) Bonnet, C. S.; Buron, F.; Caillé, F.; Shade, C. M.; Drahoš, B.; Pellegatti, L.; Zhang, J.; Villette, S.; Helm, L.; Pichon, C.; Suzenet, F.; Petoud, S.; Tóth, É. *Chem.—Eur. J.* **2012**, *18*, 1419−1431. (c) Li, Y.; Zhang, S. S.; Song, D. *Angew. Chem., Int. Ed.* **2013**, *52*, 710−713.

(6) Poole, R. A.; Montgomery, C. P.; New, E. J.; Congreve, A.; Parker, D.; Botta, M. *Org. Biomol. Chem.* **2007**, *5*, 2055−2062.

(7) Eliseeva, S. V.; Bünzli, J.-G. G. *Chem. Soc. Rev.* **2010**, *39*, 189−227.

(8) Binnemans, K. *Chem. Rev.* **2009**, *109*, 4283−4374.

(9) (a) Varlan, M.; Blight, B. A.; Wang, S. *Chem. Commun.* **2012**, *48*, 12059−12061. (b) Yamaguchi, S.; Akiyama, S.; Tamao, K. *J. Am. Chem. Soc.* **2001**, *123*, 11372−11375. (c) Wade, C. R.; Broomsgrove, A. E. J.; Aldridge, S.; Gabbaï, F. P. *Chem. Rev.* **2010**, *110*, 3958−3984. (d) Jäkle, F. *Chem. Rev.* **2010**, *110*, 3985−4022.

(10) (a) Seward, C.; Hu, N.-X.; Wang, S. *Dalton Trans.* **2001**, 134−137. (b) Feng, X.; Ling, X.-L.; Liu, L.; Song, H.-L.; Wang, L.-N.; Ng, S.-W.; Su, B. Y. *Dalton Trans.* **2013**, *42*, 10292−10303.

(11) (a) Peng, H.; Stich, M. I. J.; Yu, J.; Sun, L.-N.; Fischer, L. H.; Wolfeis, O. S. *Adv. Mater.* **2010**, *22*, 716−719. (b) Sager, W. F.; Filipescu, N.; Serafin, F. A. *J. Phys. Chem.* **1965**, *69*, 1093−1100. (c) Bender, J. L.; Shen, Q.-D.; Fraser, C. L. *Tetrahedron* **2004**, *60*, 7277−7285. (d) Bender, J. L.; Corbin, P. S.; Fraser, C. L.; Metcalf, D. H.; Richardson, F. S.; Thomas, E. L.; Urbas, A. M. *J. Am. Chem. Soc.* **2002**, *124*, 8526−8527. (e) Izatt, R. M.; Fernelius, W. C.; Haas, C. G., Jr.; Block, B. P. *J. Phys. Chem.* **1955**, *59*, 170−174.

(12) (a) Xu, S.; Evans, R. E.; Liu, T.; Zhang, G.; Demas, J. N.; Trindle, C. O.; Fraser, C. L. *Inorg. Chem.* **2013**, *53*, 3597−3610. (b) Zhang, G.; Lu, J.; Fraser, C. L. *Inorg. Chem.* **2010**, *49*, 10747−10749. (c) Chow, Y. L.; Johansson, C. I.; Zhang, Y.; Gautron, R.; Yang, L. I.; Rassat, A.; Yang, S.-Z. *J. Phys. Org. Chem.* **1996**, *9*, 7−16. (d) Kumar, R. G.; Thilagar, P. *Dalton Trans.* **2014**, *43*, 3871−3879.

(13) (a) Palmer, G. M.; Fontanella, A. N.; Shan, S.; Hanna, G.; Zhang, G.; Fraser, C. L.; Dewhirst, M. W. *Nat. Protoc.* **2011**, *6*, 1355−1366. (b) Fraser, C. L.; Zhang, G. *Mater. Today* **2009**, *12*, 38−40. (c) Zhang, G.; Chen, J.; Payne, S. J.; Kooi, S. E.; Demas, J. N.; Fraser, C. L. *J. Am. Chem. Soc.* **2007**, *129*, 8942−8943.

(14) Blight, B. A; Ko, S.-B.; Lu, J.-S.; Smith, L. F.; Wang, S. *Dalton Trans.* **2013**, *42*, 10089−10092.

(15) (a) Sakai, A.; Tanaka, M.; Ohta, E.; Yoshimoto, Y.; Mizuno, K.; Ikeda, H. *Tetrahedron Lett.* **2012**, *53*, 4138−4141. (b) Tanaka, M.; Ohta, E.; Sakai, A.; Yoshimoto, Y.; Mizuno, K.; Ikeda, H. *Tetrahedron Lett.* **2013**, *54*, 4380−4384.

(16) (a) D'Aléo, A.; Picot, A.; Beeby, A.; Williams, J. A. G.; Le Guennic, B.; Andraud, C.; Maury, O. *Inorg. Chem.* **2008**, *47*, 10258. (b) D'Aléo, A.; Pointillart, F.; Ouahab, L.; Andraud, C.; Maury, O. *Coord. Chem. Rev.* **2012**, *256*, 1604. (c) Latva, D.; Takalo, H.; Mukkala, V.-M.; Matachescu, C.; Rodríguez-Ubis, J. C.; Kankare, J. *J. Lumin.* **1997**, *75*, 149. (d) Crosby, G. A.; Alire, R. M.; Whan, R. E. *J. Chem. Phys.* **1961**, *34*, 743−748.

(17) Shi, J.; Hou, Y.; Chu, W.; Shi, X.; Gu, H.; Wang, B.; Sun, Z. *Inorg. Chem.* **2013**, *52*, 5013−5052.

(18) Gutierrez, F.; Tedeschi, C.; Maron, L.; Daudey, J. P.; Poteau, R.; Azema, J.; Tisnès, P.; Picard, C. *Dalton. Trans.* **2004**, 1334−1347.

(19) *Gaussian09*, revision B.01; Frisch, M. J.; Trucks, G. W.; Schlegel, H. B.; Scuseria, G. E.; Robb, M. A.; Cheeseman, J. R.; Scalmani, G.; Barone, V.; Mennucci, B.; Petersson, G. A.; Nakatsuji, H.; Caricato, M.; Li, X.; Hratchian, H. P.; Izmaylov, A. F.; Bloino, J.; Zheng, G.; Sonnenberg, J. L.; Hada, M.; Ehara, M.; Toyota, K.; Fukuda, R.; Hasegawa, J.; Ishida, M.; Nakajima, T.; Honda, Y.; Kitao, O.; Nakai, H.; Vreven, T.; Montgomery, J. A.; Peralta, Jr. J. E.; Ogliaro, F.; Bearpark, M.; Heyd, J. J.; Brothers, E.; Kudin, K. N.; Staroverov, V. N.; Keith, T.; Kobayashi, R.; Normand, J.; Raghavachari, K.; Rendell, A.; Burant, J. C.; Iyengar, S. S.; Tomasi, J.; Cossi, M.; Rega, N.; , N.; Millam, J. M.; Klene, M.; Knox, J. E.; Cross, J. B.; Bakken, V.; Adamo, C.; Jaramillo, J.; Gomperts, R.; Stratmann, R. E.; Yazyev, O.; Austin, A. J.; Cammi, R.; Pomelli, C.; Ochterski, J. W.; Martin, R. L.; Morokuma, K.; Zakrzewski, V. G.; Voth, G. A.; Salvador, P.; Dannenberg, J. J.; Dapprich, S.; Daniels, A. D.; Farkas, O.; Foresman, J. B.; Ortiz, J. V.; Cioslowski, J.; Fox, D. J.; Gaussian, Inc.: Wallingford, CT, 2010.

(20) (a) Lee, C.; Yang, W.; Parr, R. G. *Phys. Rev. B: Condens. Matter Mater. Phys.* **1988**, *37*, 785−789. (b) Becke, A. D. *J. Chem. Phys.* **1993**, *98*, 5648−5652.

(21) *SHELXTL*, version 6.14; Bruker AXS: Madison, WI, 2003.